THE PENNSYLVANIA STATE UNIVERSITY
SCHREYER HONORS COLLEGE

DEPARTMENT OF MECHANICAL AND NUCLEAR ENGINEERING

A COMPUTATIONAL ANALYSIS OF THE BIOMECHANICS OF IMMEDIATELY LOADED DENTAL IMPLANTS

RYAN SHANNON
SPRING 2017

A thesis
submitted in partial fulfillment
of the requirements
for a baccalaureate degree
in Mechanical Engineering
with honors in Mechanical Engineering

Reviewed and approved* by the following:

Jing Du, PhD.
Assistant Professor of Mechanical Engineering
Thesis Supervisor

Sean Brennan, PhD.
Professor of Mechanical Engineering
Honors Adviser

* Signatures are on file in the Schreyer Honors College.

ABSTRACT

Stresses and strain in the bone surrounding a dental implant are of interest regarding the study of bone healing following the dental implantation procedure. Techniques for mapping strain in bone have been developed for physical experimentation, but computational methods for finding these strain maps are more desirable for their flexibility in dealing with changing physical properties, loading conditions, and geometries.

This project first aims to develop a finite element model of a surgical dental implant and two adjacent teeth. Two implants from a cadaver are scanned by a micro-CT scanner and those images are used to create two models. The first is an implant for tooth 23 and the second for tooth 26. After building the model, the implant is loaded with a pressure and the resultant stress and strain in the teeth and surrounding bone are calculated using the finite element method. The effects of element size are studied. Various boundary conditions are explored. The parameters of the model are then modified to simulate various conditions including differences in the stiffness of the cortical bone, the teeth dentin, and the titanium implant. These differences in material properties arise from an interval of stiffness values in the literature for bone and teeth, and the unknown composition of the implant.

The computational model is compared to a physical experiment during which the same implants were loaded by a downward force of 100 N. In the experiment, the implant-tooth complexes were scanned again after loading, and digital volume correlation methods were measured to calculate the strain [1]. The goal for this project is to evaluate the finite element method as a means for studying the mechanical effects of loaded implants in the surrounding bone. The methods developed in this project might be used in future studies of implant-bone complexes.

TABLE OF CONTENTS

LIST OF FIGURES

LIST OF TABLES

ACKNOWLEDGEMENTS

I would like to thank Dr. Jing Du for all her support and mentorship with the writing of this thesis. Next, I would like to thank Dr. Gregory Lewis and Dr. Hwa Bok Wee in the Penn State College of Medicine for their assistance with technical discussions on voxel-based modeling. I would also like to thank Mr. Qiyuan Mao and Mr. Kangning Su for their technical advice relating to this project. Next, I would like to thank Dr. Reuben Kraft for sparking my interest in biomechanics and his mentorship in my first two years of undergraduate study. I would also like to thank Dr. Sean Brennan for his support as my honors advisor and secondary thesis reader. Finally, I would like to thank my parents and brothers for all their support throughout my undergraduate degree.

Chapter 1

INTRODUCTION

The most common method for testing dental implant materials and design is experimental trial. More recently (21st century) as dental implants have become a more popular as a treatment option in dentistry [2], implants have been researched more in the laboratory setting and with computer simulation. Computational models are particularly useful in this field. Dental implants have many variables for evaluating effectiveness. Some of these variables are implant material, implant geometry, and tooth socket geometry.

The variability of the tooth-implant complex has been a point of study for computational biomechanics. A challenge for studying the mechanical properties of this area is the creation of a detailed and accurate model. The first portion of the report details the methods used to create 3-D models from CT scans of two tooth implant complexes from a human cadaver.

Studying the strain in the bone surrounding the implant is of interest. The strain in this area of a healthy tooth-bone complex is different from that of an implant-bone complex. The loading and resulting strain of the bone and surrounding tissue directly effects the repair and reformation of the bone and tissue [3]. Analyzing the strain in this area is therefore important for understanding this healing process.

The model is compared to a physical experiment previously performed on the same specimens. In this experimental study, the implants were loaded and the strain in the implants was mapped by correlating 3D images of the specimen before the loading with images obtained after the loading [1]. The primary comparison will be the values of strain obtained from experimentation and those calculated in the model. The comparison is performed to validate this method as a means for calculating strain in the alveolar bone that surrounds an implant.

The goal for this project is to find a means for the development of a finite element model of the implant-bone complex. After comparing the model to the physical experiment, changes to material properties on the implant-bone complex are simulated to study the effect these changes have on the strain experienced in the bone surrounding the implant. The ability of the model to describe the bone's response to different material properties and loading is important for the bone's repair and reformation. Therefore, a good model should be able to capture changes in the bone's response due to changing model parameters.

Chapter 2

BACKGROUND

2.1 Overview of Teeth Anatomy

The crown of a tooth consists of three biological materials. The outermost layer is enamel, a very hard material consisting mostly of minerals. Beneath enamel is dentin, a material softer than enamel consisting of a smaller percentage of minerals and higher percentages of organic materials and water. The innermost layer of the crown is made up of pulp, an extremely soft material composed primarily of soft tissue. Tooth decay that reaches the pulp can be extremely painful as this area contains nerve cells.

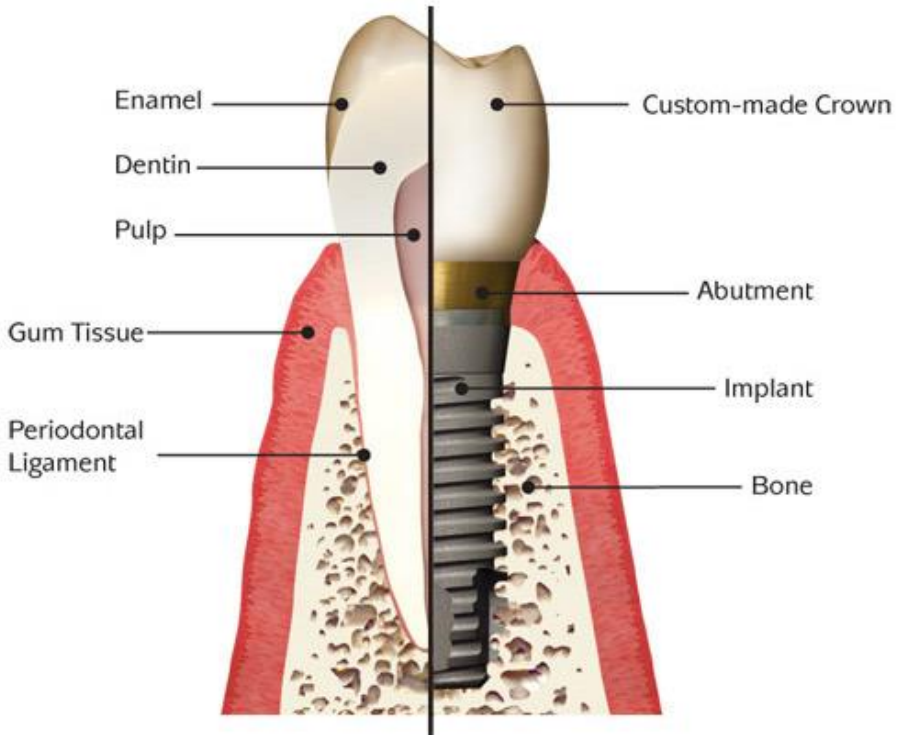

Figure 1: The Structure of a Tooth and Implant [4]

The root of the tooth is surrounded by gum, bone, the periodontal ligament and extensions of the dentin and pulp from the crown. The gum is a layer of soft tissue that lines the mouth. The bone is thicker in the exterior (cortical bone) with increasing porosity inwards (trabecular bone). The periodontal ligament is a very thin layer of connective tissue between the bone and dentin [4].

Finally, the surfaces of the bone are described as buccal, lingual, mesial and distal. The buccal surface is the outward facing surface (part of tooth one show's when smiling) and the lingual is the opposite surface, the inside surface of the tooth. The mesial and distal surfaces are the sides of the teeth (portions you insert floss). The mesial surface is the portion of the tooth closer to the front of your mouth and the distal is closer to the back of your mouth.

2.2 How Loading Effects Bone

Micromovement of the implant and bone under load relating to the bone's microstructure and physical properties is a new area of study. Recent findings regarding tooth implants have concluded that loading and the resulting strain in bone has effects on the bone's ability to repair and reform. These studies also suggest the bone naturally adapts its structure until optimal levels of strain are achieved [3].

Upon the removal of a tooth and replacement with an implant, the geometry of the bone surrounding the implant (formerly tooth) drastically changes. The repair process then begins to take place in the bone with strain levels varying until the optimal strain levels are achieved again. The ability of an implant to facilitate this process is of interest, as it follows that optimal bone repair is achieved with strain distributions that are most comparable to the natural strain exhibited in healthy bone.

2.3 Types of Implants

Implant design, from geometry to materials to surface finish, has been a growing field of study during the last 25 years. It is estimated that there are currently over 1300 types of dental implants on the market today [5]. The focus of the most recent research is the chemical and mechanical properties of implants, but different geometries also have advantages in particular situations.

The surface finish of dental implants has been formalized since the 1980s. A rough surface finish has been proven to provide a better micromechanical locking as well as a more effective osseointegration (the formation of a direct interface or connection between the bone and the implant). The rough surface enables greater bone-implant contact area improving implant stability and increasing interaction between the implant's chemical properties and surface coatings with the bone [6].

Implants with chemical properties of high surface energy and high wetting capability have been shown to increase the ability of the implant to absorb proteins, helpful for osseointegration. Surface coatings might include delay-release tetracycline, ibuprofen and/or calcium phosphate. The tetracycline and ibuprofen encourage tissue integration and the calcium phosphate improves mineral deposition leading to better long-term implant stability [7].

There are two basic types of implant geometry: threaded and press fit. Threaded implants perform better for longer length implants, in dense bone, and for immediately loaded implants. Thread pitch, thread geometry, helix angle, and other factors commonly associated with screws may have an impact on implant stability. These effects are still being studied. Press fit implants are more effective for shorter lengths and in more porous areas of bone [5].

Figure 2: Types of Dental Implants [8] **Threaded (left), Press-fit (middle-right), and Combination (far-right)**

The materials used in dental implants have varied from the beginning of implant dentistry in the mid 1930's until present. From polymers, cobalt-chromium allows, and iron-chromium-nickel alloys in the 20th century to ceramics (i.e. zirconia), titanium, titanium-vanadium alloys, and titanium-zirconium alloys in the 21st century, numerous materials have been tested to find high strength and low corrosion material properties suitable for tooth replacement [2].

2.4 Testing Implant Effectiveness

Testing for the effectiveness of implants is challenging and there are a multitude of both physical and computational tests. One of the most common physical test is the torque test, but resonant frequency analysis, periotests, and strain gauges are also used. Computational methods including the finite element method, digital volume correlation (DVC) and digital image correlation (DIC) have also been used to describe the biomechanics of the bone-implant complex.

Measurement of installation torque and removal torque provides information about the initial stability of a dental implant. The torque required to install an implant can be measured using an electronic torque controller and recording the peak torque value. One hour after implant placement, the implant can be removed to gauge initial implant stability. The peak removal torque is less than the peak insertion

torque, and their values can be used to assess the quality of bone surrounding the implant and the implant's ability to establish initial stability [9].

The resonant frequency test and periotest are similar methods to measure implant stability by tapping the implant and measuring the resulting movement. The resonant frequency test is performed by placing a metallic transducer on the implant and striking the implant. Measuring the frequency of the implant's vibration can give an estimate for implant stability. The resonant frequency test is popular, as it is non-invasive, can be performed immediately after placement to measure initial stability and repeated at later times to monitor the healing process. The periotest involves a metal slug and accelerometer attached to the end of a probe. The slug strikes the implant, and the contact time between the slug and implant is used to measure implant mobility. This test can be sensitive to implant angulation and surface variations of the implant in the area struck [9].

Measuring the strain in the area surrounding the implant has become popular because of its correlation to bone repair and reformation. Strain measurements from strain gauges has also been proven to correlate to peak insertion and removal torque [10]. Physically, strain gauges can be attached to the area around the implant and strain can be measured under load, however the initial gauge length will affect the reported strain values. The interest in calculating strain in the bone surrounding the implant has given arise to the use of computational analysis to find strain.

The finite element method, digital volume correlation, and digital image correlation have all been used to investigate the interaction between implant and bone [3]. This project aims to develop and finite element model using voxel-based meshing and to compare its results to a study of the same samples that uses digital volume correlation to calculate strain [1].

Chapter 3

METHODS

3.1 Model Creation

Two meshing methods were attempted to model the bone-implant complex. The first used tetrahedral-based meshing techniques in Avizo 9.0.1 and was unsuccessful. The second used voxel-based meshing techniques and was successful and used for simulation.

3.1.1 Avizo Tetrahedral-Based Mesh Generation

Initial efforts to create a mesh of the implant-teeth complex utilized the automatic mesh creating tools available in Avizo 9.0.1. Avizo uses an in-house meshing algorithm to form a tetrahedral-based model. Several meshes were generated using this software and attempts were made to modify them so that they could become suitable for simulation.

Avizo's method for creating a mesh begins with the creation of a mesh surface. After a surface is created, a number of checks are run to ensure the surface does not intersect with itself and that the orientation of the surface normal does not change in the mesh. After the surface passes the surface-quality tests, a grid of points is generated for the surface and within the surface. This grid of points is used to define the boundaries of the tetrahedral elements of the final mesh. Once the grid is generated, further tests are conducted to check the element quality. Element quality checks include an aspect ratio test and a hole test. The aspect ratio test determines if there are elements that have large lengths compared to widths (appear skinny). The hole test checks for breaks in the 3D mesh structure. Holes in the mesh and elements

with high aspect ratios are undesirable as they are likely to cause errors when the model is loaded during simulation.

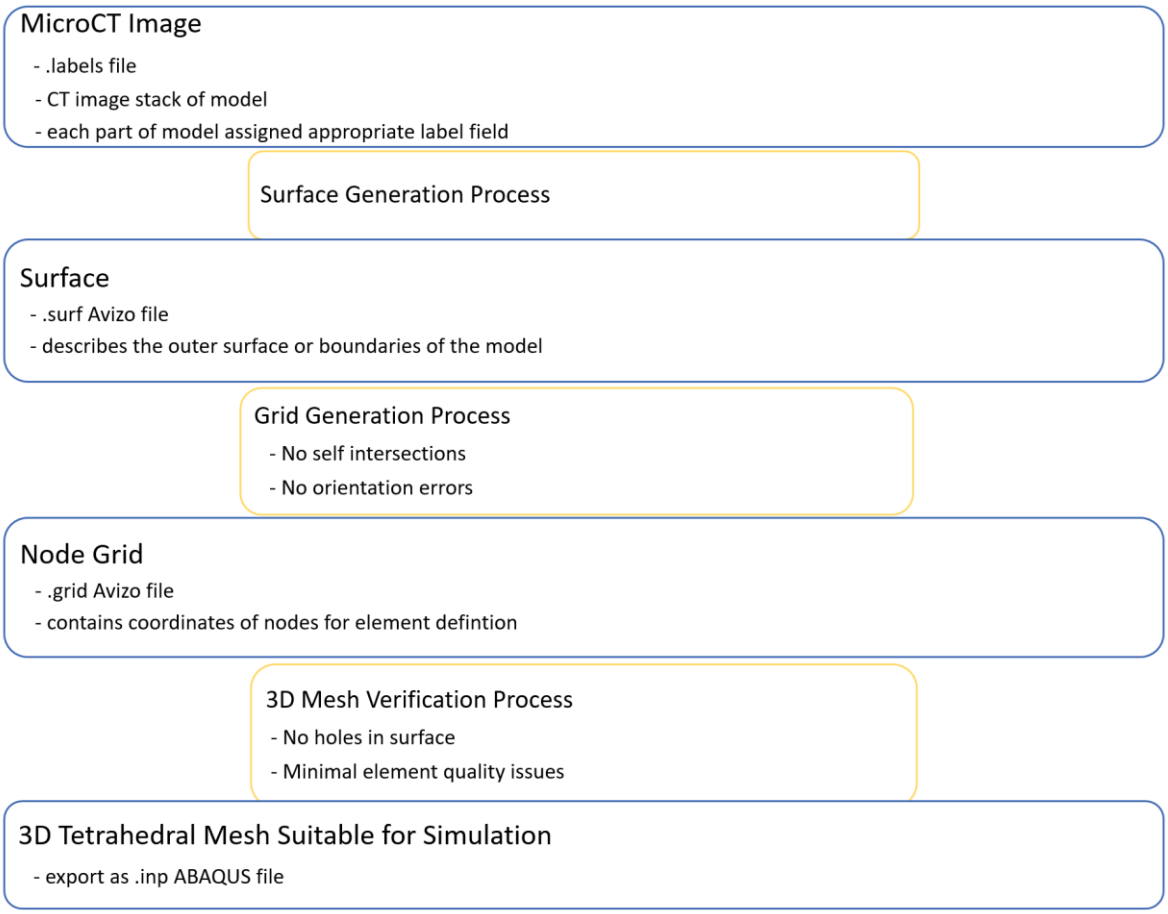

Figure 3: Tetrahedral Mesh Creation Flow Chart

As shown in Table 1, none of the meshes generated using this method were viable for further simulation. Table 1 specifies the parameters used within Avizo to create ten tetrahedral meshes. Initially, the target surface size was 100,000 surface element faces. The meshes created with this surface element target (meshes 1-4) resulted in many surface meshes with self-intersections. Surfaces with self-intersections are unable to be used for grid generation. Mesh attempt 4 had the least number of

intersections, so the parameters used in this attempt, particularly “Create Level of Detail” and “Intersection Test Strategies” were used for future attempts.

After the basic model parameters were chosen, the number of surface elements was increased in the hope of obtaining a model with fewer intersections. Mesh attempt 5 resulted in a surface with only one intersection are therefore was chosen as a viable option to proceed to grid generation. The singular intersection was manually removed by dragging a node to a new position such that the model did not intersect. After passing the intersection and orientation tests, attempt 5 proceeded to grid generation. The Avizo algorithm was unable to complete an adequate grid generation and returned an error with a suggestion to increase number of surface elements.

Mesh attempts 6-9 were similar to attempt 5. The generated surface had few intersections that were able to be removed manually, and the surface was passed onto the grid generation step. The grid generation returned errors until the number of surface elements was increased to one million in attempt 10.

This final grid generation returned a 3D mesh with approximately 2.5 million tetrahedral elements. Although the mesh was finally able to be generated by the software, this mesh was ultimately rejected as appropriate for this study. The first reason for rejection was that the total number of elements (2.5 million) was very large. Our previous experience with ABAQUS models indicates that the models for simulation should be kept under 2 million elements. Models larger than this tend to create errors in the software when simulated. Additionally, 40 elements failed our aspect ratio test, an indicator for poor element quality. With these two concerns for the model to run simulations successfully, the tetrahedral-based meshing tool was abandoned and another meshing method was pursued for model creation.

Table 1: Tetrahedral Mesh Generation Parameters

Meshing Attempt #	Target Faces	Max Dist.	Min Dist.	Finish Faces	Intersections	Orientation Problems	Preserve Slice Structure	Fast Generation
1	100000	3	0	99130	19	0	NO	NO
2	100000	3	0	99130	19	0	NO	NO
3	100000	3	0	99138	19	0	NO	NO
4	100000	3	0	99148	13	0	NO	NO
5	250000	3	0	249752	1	0	NO	NO
6	260000	3	0	259772	2	0	NO	NO
7	400000	0	0	299848	2	0	NO	NO
8	500000	3	0	499872	2	0	NO	NO
9	500000	3	1	499872	2	0	NO	NO
10	1000000	3	0	999902	0	0	NO	NO
Meshing Attempt #	**Create Level of Detail**	**Holes**	**Tetra Aspect Errors**	**Intersection Tests Strategies**	**Grid Generation**	**Nodes**	**Triangles**	**Tetrahedrons**
1	NO	NA	NA	NO	No Attempt			
2	YES	NA	NA	NO	No Attempt			
3	NO	NA	NA	YES - Med Planar Test	No Attempt			
4	NO	NA	NA	YES - Extensive Planar Test	No Attempt			
5	NO	NA	NA	YES - Extensive Planar Test	Unsuccessful			
6	NO	NA	NA	YES - Extensive Planar Test	Unsuccessful			
7	NO	NA	NA	YES - Extensive Planar Test	Unsuccessful			
8	NO	NA	NA	YES - Extensive Planar Test	Unsuccessful			
9	NO	NA	NA	YES - Extensive Planar Test	Unsuccessful			
10	NO	0	40	YES - Extensive Planar Test	Succeeded but quality warning	671,744	5,498,251	2,499,150

3.1.2 Mimics Voxel-Based Mesh Generation

The second method used for model meshing was voxel-based meshing. Instead of forming tetrahedral shaped elements, voxel meshing uses cubic or sometimes called "brick" elements. This type of mesh lends itself to image-based meshing because 3D micro-CT images are comprised of voxels (similar to the pixels in 2D images). The drawback of voxel-based meshing is that the resultant model's surface is not as smooth as a tetrahedral-based mesh. We believe the detail of the model is great enough to combat the limits to the model's surface smoothness.

In order to obtain a voxel-based mesh, we utilized the assistance of Dr. Gregory Lewis from the Orthopedics and Rehabilitation Department at Penn State Hershey. Dr. Lewis' lab has used Mimics 18.0 before in modeling the humeral head in the human shoulder. With his assistance, we were able to create three voxel-based models from our CT scans. The Mimics software converted the label fields of our segmented CT scans to ABAQUS input files. The separately segmented labels were then each assigned to their own material property, thereby defining which part of the scan was bone, tooth, implant, or space. Finally, the input files were imported to ABAQUS for simulation.

The original micro-CT scans have a resolution of 25 μm. Using a 1:1 ratio for the image resolution to the model resolution would result in voxel-element numbers much too large for ABAQUS. The detail of the mesh was a desired testing parameter, so Mimics was used to create two meshes for implant complex 23 of different mesh size. Only one small mesh size model was generated for complex 26. Table 2 below details the sizes of the three models created with the Mimics software. These three models were used for every simulation in this report. The models are referred to as "Coarse 23", "Fine 23", and "Fine 26".

Table 2: Voxel-Based Mesh Parameters

Model Name	Size Reduction Ratio	Final Node Number	Final Element Number
Coarse 23	343:1	435,519	346,326
Fine 23	64:1	2,344,923	1,984,700
Fine 26	64:1	2,414,672	2,020,203

All three models (Figures 4-6) have uniform element size. Future model refinement would utilize variable element size, as it allows for faster, and more accurate models. In the tooth-implant complex, the teeth are modeled as solid, and the stress/strain in the teeth is both minimal and not of interest for this study. Therefore, the teeth could be modeled with significantly larger elements, thereby reducing the total element number for each model. This reduction in the total number of elements can be beneficial in two ways. Either the model can be simulation with a smaller number of elements (making it faster) or areas of higher detail, like the implant-bone contact area, could be modeled with smaller sized elements. Higher detail in this area of interest would lead to more accurate stress/strain distributions.

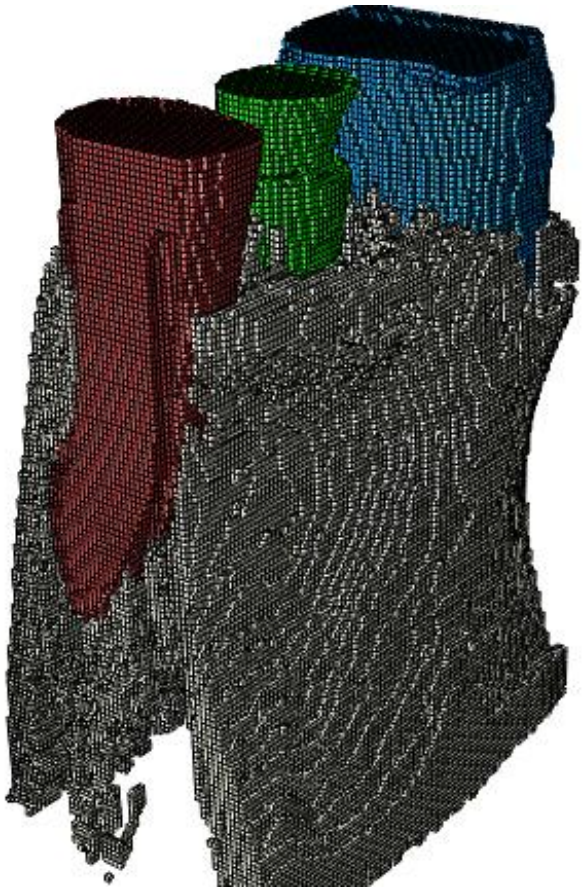

Figure 4: Coarse Tooth-Implant 23 Complex

Figure 5: Fine Tooth-Implant 23 Complex

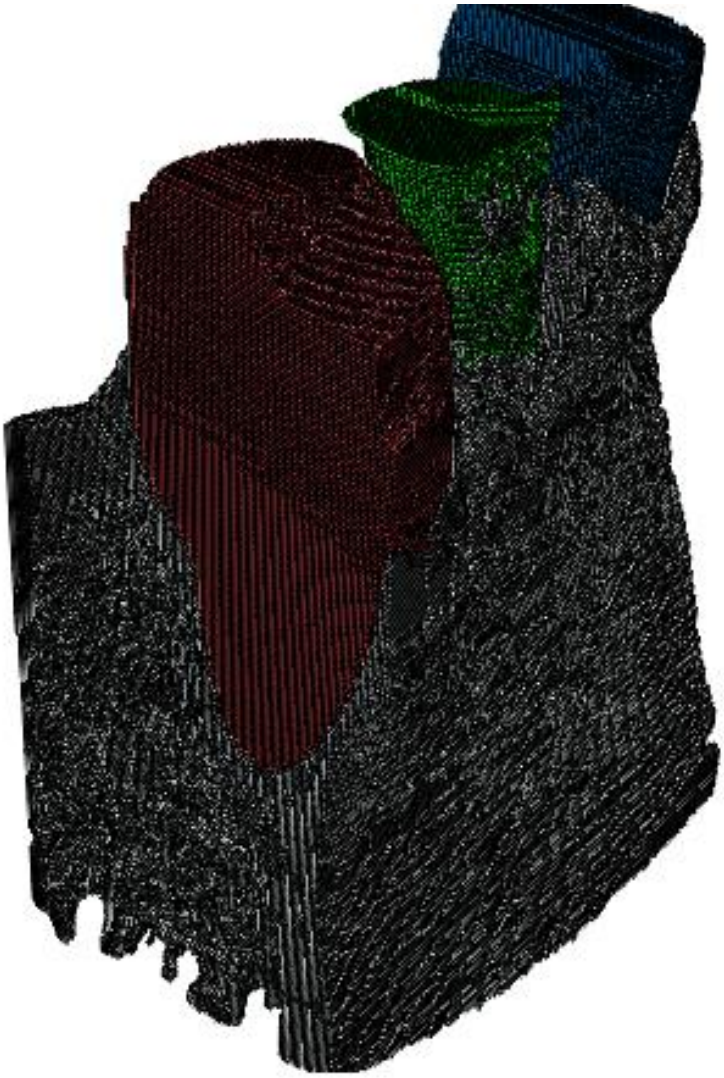

Figure 6: Fine Tooth-Implant 26 Complex

3.2 Simulation Method

All simulations were performed using ABAQUS 6.14 on the Penn State Lion-X and ISC-ACI systems hosted by the Penn State Institute for CyberScience. The simulations are single step analyses which analyze the effects of a static applied load of 100 N to the top of the implant.

The Mimics file and ABAQUS input file are written such that the entire model is a single part. Element sets are used to define the bone, teeth, and implant. There is no need to define any contact parameters because the entire model is only one part. The process for modifying the file exported from Mimics is as follows. First, the values of the material properties are assigned to each material. Then a singular "instance" is created for the entire part as different meshes are not applicable for this project. Next the boundary condition is established. A discussion of boundary conditions can be found in the results section.

The class of material in ABAQUS used in each simulation is "elastic-isotropic". The Young's modulus and Poisson's ratio are defined for each of these properties. The value for the bone and the teeth are from literature (see Table 3). The material properties of the titanium implant used (Straumann ® Roxolid ®, BL, Ø 4.1 mm RC, SLActive ® 14 mm, TiZr, Institut Straumann AG, Basel, Switzerland) are proprietary to the company, so a range of titanium alloy implants were used in this study.

Table 3: Material Properties Used in ABAQUS Simulation

Material	Young's Modulus (GPa)	Poisson's Ratio	Citation
Bone	15-25	0.30	[11], [12]
Tooth	15-18.6	0.31	[13]
Implant	90-116	0.34	[14]

The model uses the material properties comparable to that of cortical bone. The model includes the detail of the trabeculae within the bone, and therefore the bone is given the material properties of dense, cortical bone. Anisotropy is neglected as a material property, but the range of stiffness for bone reflects the effective stiffness at different directions for anisotropic cortical bone. Also, the anisotropy for trabecular bone is reflected in the anisotropic microstructures in our model.

The entire tooth is modeled with a singular material property. The selection of this material property is related to the material properties of dentin. The dentin layer is larger than the layer of pulp and significantly larger than the periodontal ligament. These three materials were therefore modeled as a single material whose material properties were in the range of dentin and less stiffness than dentin, to account for the softer pulp and periodontal layers.

An additional step is then added to the initial step. This new step has two uses. First, it is defined identically to the initial step and the model is run through a datacheck. The datacheck is a way for ABAQUS to check that all model parameters have been defined appropriately. Datacheck is also used in the models to identify unconnected regions in the model. Mimics does not check that its exported model is connected as one piece. The datacheck step reports any unconnected regions in the model. The unconnected nodes are then given their own boundary condition that fixes them in place to prevent any rigid body movement.

After the datacheck analysis is performed, the secondary step is modified such that the initial boundary condition remains, but additionally a load is applied to the top of the implant. The load applied is a uniform pressure load. ABAQUS has an option for the user to input the desired total force applied to

a surface. This total load was set to be 100 N. Uniform pressure is selected as the loading type as it is thought to best simulate the condition of the physical experiment the model is compared against. The physical experiment used a tensile/compression stage that first applied load to a composite connected to the top of the implant [1].

With the boundary conditions, material properties, and loading conditions set, the model is ready for simulation. The models were simulated on both the Lion-X and ACI-ISC systems at The Pennsylvania State University. The simulations were run on one node at 16 processors per node and physical memory size of 30 GB. The length of the simulation was about 10 minutes for the “Coarse 23” model. The length of the “Fine 23” and “Fine 26” models were about 3 hours. The drastic increase in time is due to the increase in element number between the coarse and fine models.

Chapter 4

RESULTS AND DISCUSSION

This section discusses the parameters tested in each simulation so that each parameter's effect might be studied. Each section details which parameter was changed, why the parameter might affect the result, and the resultant changes in the model's simulation. The results are compared to the experimental data obtained previously and the chapter concludes with a discussion of proposed further study.

4.1 Effects of Element Size

Element size is one of the limiting factors for a model when it comes to accuracy. As mentioned earlier in this report, a finite element mode increases in accuracy as the element size decreases until the model converges to a solution, at which point the further reduction in the element size does not affect the results. Developing a model with larger element sizes is desirable because those models have a smaller total number of elements. With less elements, less calculation is required for a solution, and therefore those solutions are achieved more quickly. However, if this faster model does not provide an accurate solution, a slower model should be used.

Ideally a model can be re-meshed easily to create a number of models with various element sizes. Simulating all the models would allow for a determination of the converged solution and the largest element size that reaches that solution. Any further changes to the model would then also be simulated with the determined element size. Given the effort, travel, and time required for this project's meshing, only two element sizes were created for the Implant 23 complex, and only one for the Implant 26 complex. The meshing process is one of the most desirable parts of this project to improve, and further developments of this project might focus on the ability to more easily generate meshes of implant-bone complexes.

The two meshes for the implant 23 complex are described as the “Coarse 23” and the “Fine 23”. The coarse mesh reduced the size of the CT scan by grouping 343 voxels (a 7x7x7 cube) and assigning that element to either implant, bone, tooth, or empty space. The resultant mesh modeled the complex with 346,326 elements. The fine mesh reduced the size of the CT scan by grouping 64 voxels (a 4x4x4 cube) to one element. The resultant fine mesh was 1,984,700 elements.

These two models were simulated using a 100 N load, bone stiffness equal to 15 GPa, tooth stiffness equal to 18.6 GPa, and implant stiffness equal to 116 GPa. The maximum strain differs between the two models by 2%, which is not very large, but the larger strain value occurs in the coarse model. The finite element method normally increases its maximum stress/strain value when the element size is decreased. Further investigation of the model revealed that the location of the maximum strain was different in the coarse and fine models. The fine model had the largest strain in a region where the implant contacts the bone about halfway down the length of the implant. This region where the bone contacts the implant, does not appear in the coarse model because that model does not have a connection between the implant and bone.

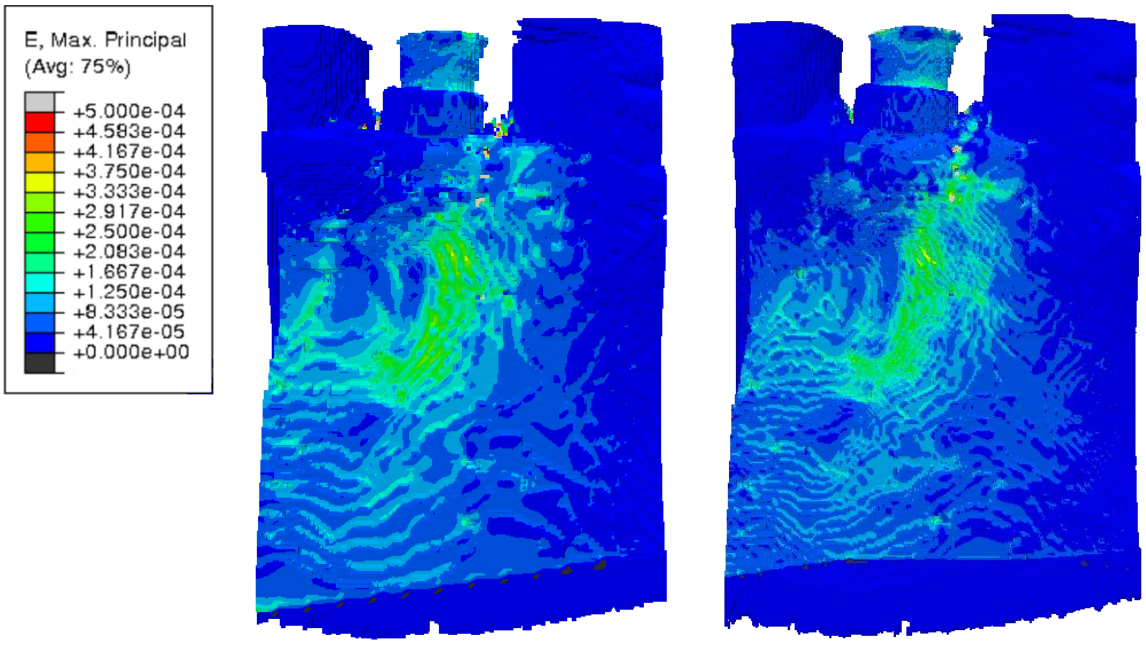

Figure 7: Buccal Strain in Coarse 23 (left) and Fine 23 (right)

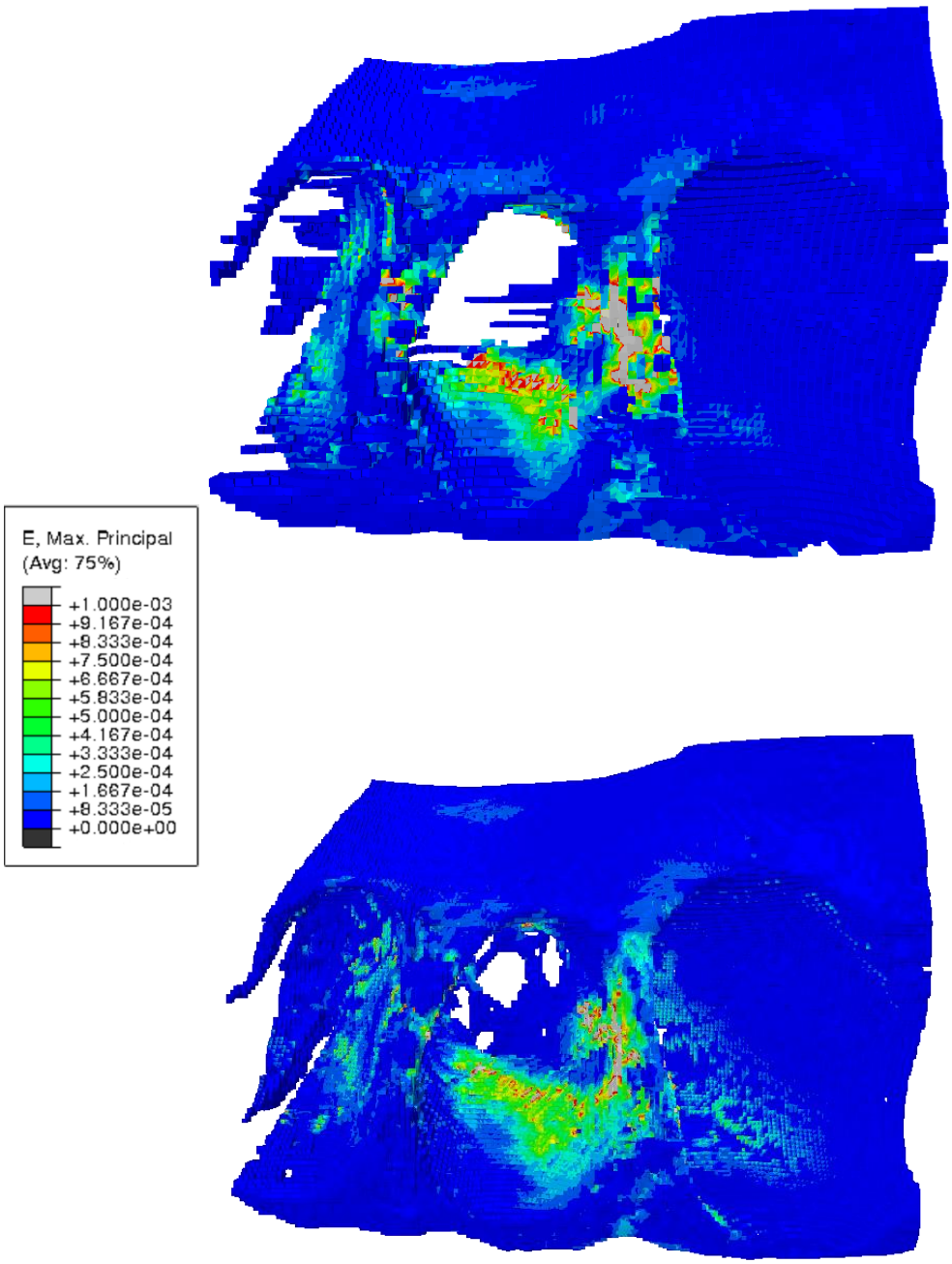

Figure 8: Implant Socket Strain (Top-View) in Coarse 23 (top) and Fine 23 (bottom)

Table 4: Effects of Element Size on Implant 23

Implant	Mesh	Bone Modulus (GPa)	Tooth Modulus (GPa)	Implant Modulus (GPa)	Buccal Strain	Max Strain	Max Strain Location	Maximum Implant Displacement (μm)
23	Coarse	15	18.6	116	0.037%	0.487%	Implant Socket, Upper	12.0
23	Fine	15	18.6	116	0.036%	0.476%	Implant Socket, Middle	10.9

4.2 Effects of Boundary Conditions

Boundary conditions are an important selection when deciding the parameters of a simulation. This project uses a relatively simple boundary condition. The bottom of the implant is fixed in all three directions and fixed in rotation. Selecting the elements or boundary at which this zero-displacement condition occurs was performed by manually selecting nodes.

By changing the number of elements selected, the effect of a small/large boundary condition was studied. In the "Fine 23" model, a small part of the model (116,900 nodes), about 10% of the total height, was fixed at the bottom of the complex. The implant was loaded and the strain was recorded below in Figure 9. The same model, with the same material conditions, was fixed using a larger boundary condition (310,986 nodes), about 17% of the height, and loaded. Comparing the results in Figure 9 shows that while the strain continues farther down the implant in the smaller boundary condition model, the strain distribution is similar. Also, the maximum strain on the buccal surface (which is of interest) is similar.

The difference in the strain occurs near the region that the boundary condition was applied. Notice the higher strain values along and near the boundary condition. The change in the boundary conditions does not significantly affect the regions of interest, however, so the selection of the boundary conditions will not significantly affect the results. The smaller boundary condition was selected for the remainder of the simulations because it provides a better picture of the strain distribution closer to the bottom of the implant. It is also believed to be a better representation of the implant-tooth complex in experiments, where the bottom of the complex is fixed in acrylic.

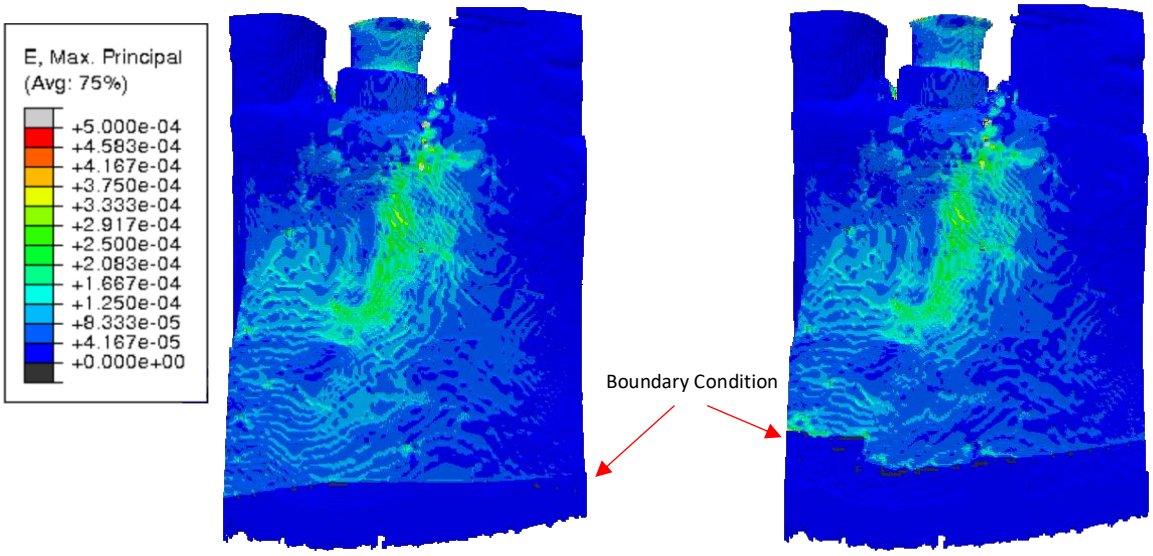

Figure 9: Fine 23 Buccal Strain, Small Boundary Condition (left) and Larger Boundary Condition (right)

4.3 Effects of Bone's Material Properties

Changes in the value of the Young's modulus of bone had the greatest effect of any variable material property. Bone with higher stiffness expectedly resulted in less movement and therefore lower strain values. The relationship between the Young's modulus of the bone and the strain on the buccal bone surface is approximately linear as shown in Figure 10. The stiffness of the bone also has a significant role in the displacement of the implant. The conditions and results of all simulations performed are recorded in Tables 5 and 6.

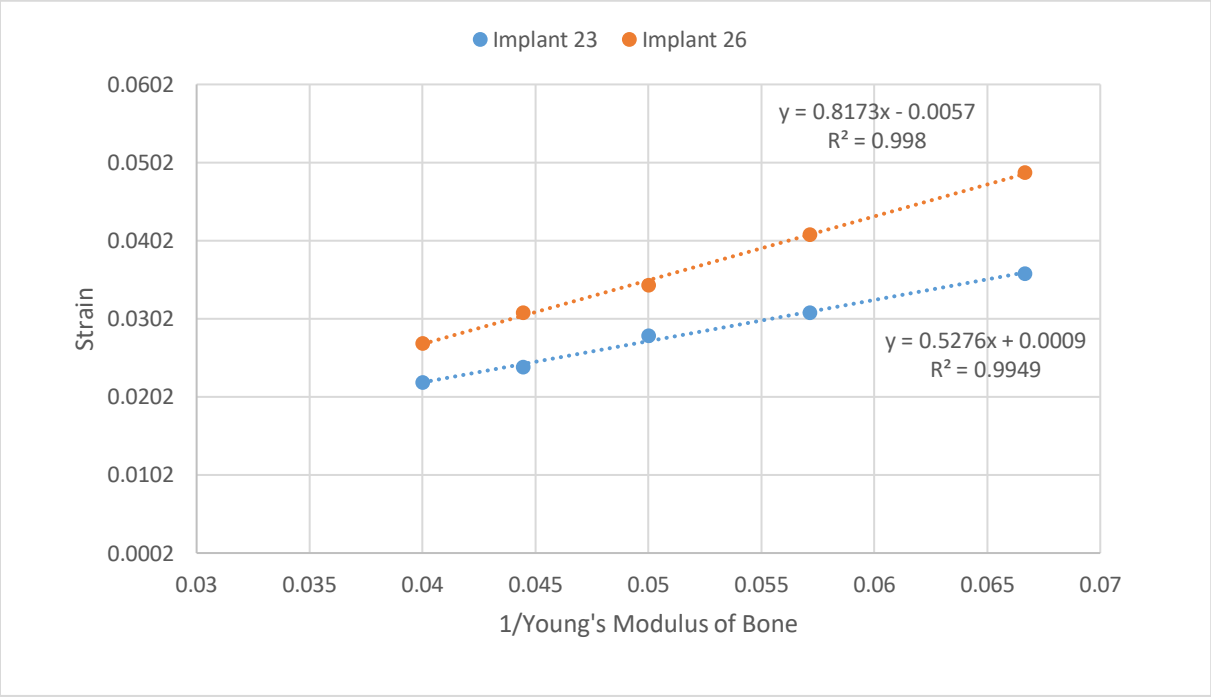

Figure 10: Linear Relationship between Strain and 1/Young's Modulus

Table 5: Effect of Bone Stiffness on Implant 23

Implant	Mesh	Bone Modulus (GPa)	Tooth Modulus (GPa)	Implant Modulus (GPa)	Buccal Strain	Max Strain	Maximum Implant Displacement (µm)
23	Fine	15	18.6	116	0.036%	0.456%	10.9
23	Fine	17.5	18.6	116	0.031%	0.402%	9.9
23	Fine	20	18.6	116	0.028%	0.348%	9.2
23	Fine	22.5	18.6	116	0.024%	0.313%	8.6
23	Fine	25	18.6	116	0.022%	0.259%	8.1

Table 6: Effect of Bone Stiffness on Implant 26

Implant	Mesh	Bone Modulus (GPa)	Tooth Modulus (GPa)	Implant Modulus (GPa)	Buccal Strain	Max Strain	Maximum Implant Displacement (µm)
26	Fine	15	18.6	116	0.049%	1.03%	18.7
26	Fine	17.5	18.6	116	0.041%	0.89%	17.1
26	Fine	20	18.6	116	0.035%	0.79%	15.8
26	Fine	22.5	18.6	116	0.031%	0.70%	14.8
26	Fine	25	18.6	116	0.027%	0.65%	13.9

4.4 Effects of Teeth/Dentin Material Properties

Variation in the stiffness of the teeth were modeled to account for the combination of dentin, periodontal ligament, and pulp as one material. The stiffness of pure dentin (18.6 GPa) was decreased to account for the softer periodontal ligament and pulp. The decrease in the tooth stiffness value did not have a significant effect on the area of interest (stain on the buccal surface) or the overall displacement of the implant. The teeth are far enough away from the implant-bone complex such that changes in their material properties do not have a great effect on the strain in the bone.

Table 7: Effect of Teeth Stiffness on Implant 23 and 26

Implant	Mesh	Bone Modulus (GPa)	Tooth Modulus (GPa)	Implant Modulus (GPa)	Buccal Strain	Max Strain	Maximum Implant Displacement (µm)
23	Fine	15	18.6	116	0.036%	0.456%	10.9
23	Fine	15	12	116	0.036%	0.456%	11.2
26	Fine	15	18.6	116	0.049%	1.026%	18.7
26	Fine	15	12	116	0.049%	1.030%	19.1

4.5 Effects of Implant Material Properties

The stiffness of the implant is unknown but can be estimated with the stiffness of titanium and titanium alloys commonly used for dental implants. Changing the stiffness of the implant had little effect on the resulting strain in the model. The top of the implant experienced more displacement, as expected, but the displacement at the middle and bottom of the implant did not change. This resulted in small changes in strain at the buccal surface.

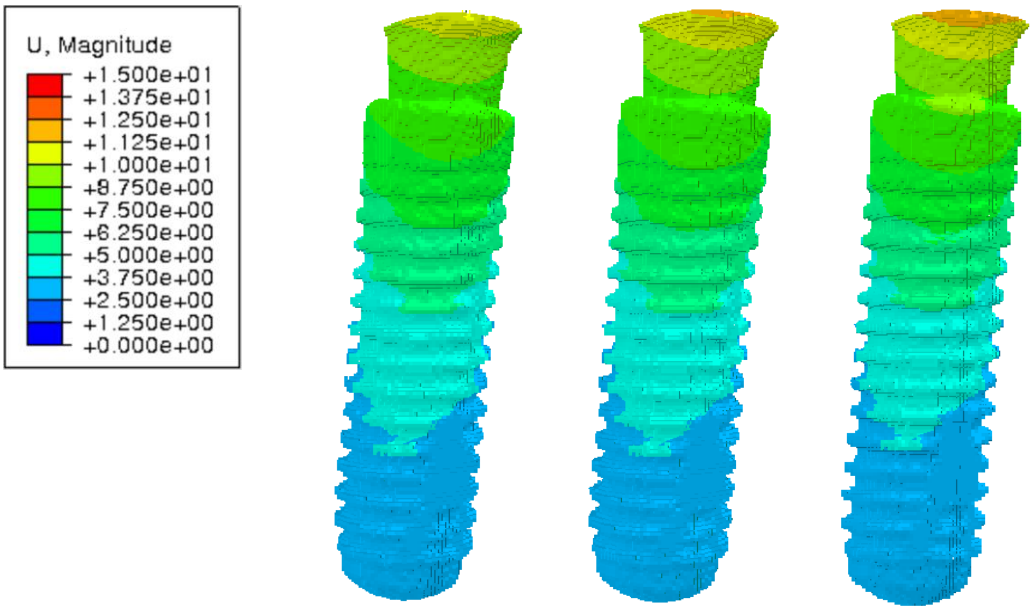

Figure 11: Displacement (μm) for Implant Stiffness 116 GPa (left), 100 GPa (middle), and 90 GPa (right)

Table 8: Effect of Implant Stiffness on Implant 23

Implant	Mesh	Cortical Modulus (GPa)	Dentin Modulus (GPa)	Titanium Modulus (GPa)	Buccal Strain	Max Strain	Maximum Implant Displacement (μm)
23	Fine	15	18.6	116	0.036%	0.476%	10.92
23	Fine	15	18.6	100	0.036%	0.450%	11.60
23	Fine	15	18.6	90	0.035%	0.467%	11.93

4.6 Comparison to Experimental Results

The finite element method predicts higher strain concentrations in the buccal bone and at the implant-bone contact areas. The results have good agreement with those obtained from micro-CT coupled experiments and digital volume correlation method reported by Du et al. [1]. The trend for strain distribution is similar on the buccal and lingual surfaces for both simulation and experimentation. Also, the highest strain values occur in the implant socket. However the strain values obtained from our finite element method are about an order of magnitude less than that of the digital volume correlation method in Du et al [1]. The DVC model reports strain values around 0.5% on the buccal surface for Implant 23 and close to 2.0% on the surface of Implant 26. The implant socket experiences strains around 2.0% in both Implant 23 and 26 from the experiment. Due to the imaging artifacts, the strain value may be overestimated in the experiments. Due to the reduced element number and simplified material properties, the strain value could be underestimated in our simulations. Tuning the model geometry and material properties are suggested in the following section and may result in results closer to those measured from experiments.

Table 9: Comparison of Implant 23 to DVC Method [1]

	Buccal Surface	Lingual Surface	Top View of Implant Socket
Finite Element	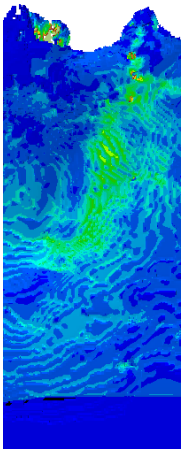	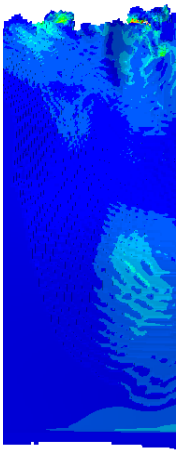	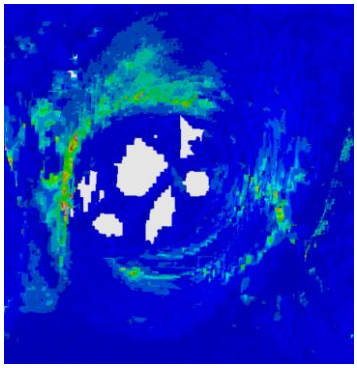
Digital Volume Correlation	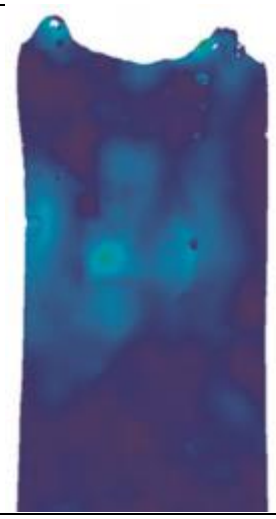	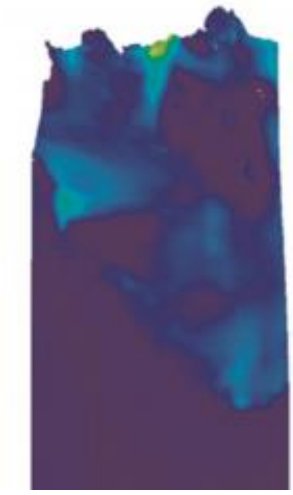	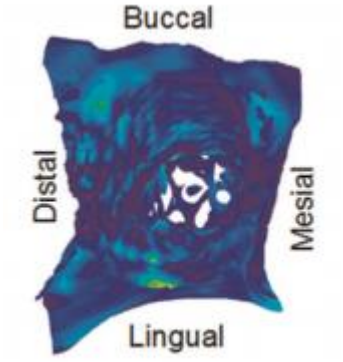

Table 10: Comparison of Implant 26 to DVC Method [1]

	Buccal Surface	Lingual Surface	Top View of Implant Socket
Finite Element	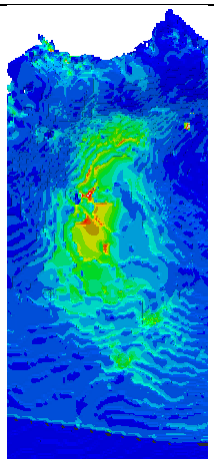		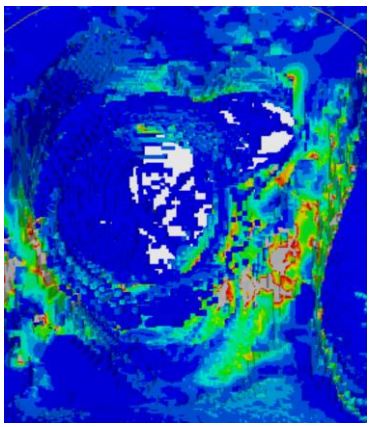
Digital Volume Correlation	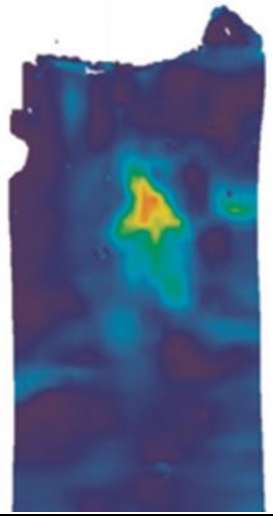	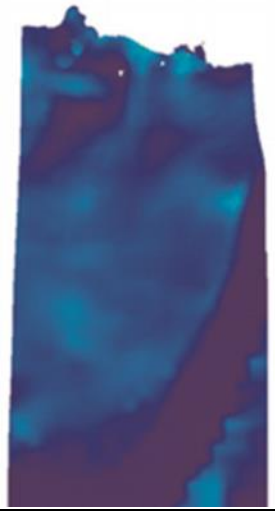	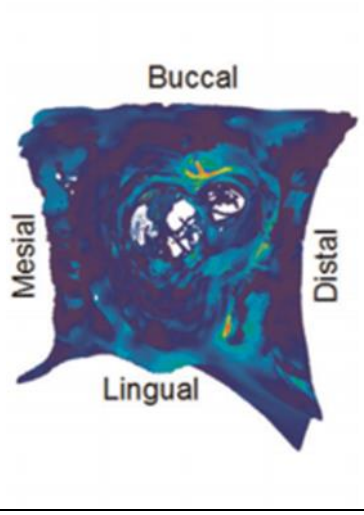

4.7 Implications and Future Work

The finite element model shows promise for future modeling of strain in the implant-bone complex. There are future developments that might be taken to improve upon the results of this report.

The first improvement might come from a more detailed mesh. There is indication that the results need to be improved. The strain values do not exactly match those found with digital volume correlation, even though the distribution is very similar. To achieve more accurate results, the mesh might be even finer. The CT scan resolution was 64 times finer, and perhaps a smaller reduction or no reduction at all would provide more accurate results. A smaller element size would be very helpful in the area where the implant contacts the bone. This is area where the implant contacts the bone and thus how the load is transferred to the bone. Creating a detailed geometry in this area is therefore very important. For this project, 2 million elements created a very large file for ABAQUS, which is why the 64 times reduction was necessary. However, this project used uniform element size for the entire model. The teeth on either side of the implant are not porous though, and the results of section 4.4 suggest that the material properties in this outer region has very little effect on the area of interest. The first suggestion of this report would be to create a new mesh with varying element size, using large element for the teeth and small elements for the contact area between implant and bone, thus enabling the total mesh size to remain near 2 million elements.

The material property of the bone is another area that needs further study. This property had the highest influence on the resultant strain of any of the variables tested. However, these material properties were approximated and a wide range needed to be tested to account for neglecting anisotropy. The next suggestion for this project would to investigate methods for modeling the anisotropy of the cancellous bone surrounding the implant.

The third suggestion is for an evaluation of the bone-contact area for each of the models. There is a very small difference between the Coarse 23 and Fine 23 models. The coarse model even has higher strain values than the fine model which would not occur if the two models had the same geometry. There

is a significant difference in the geometry of the two models in the implant-bone interface. This difference is great enough to cause unusual results. The third proposal for further study is to calculate the implant-bone contact area for all three models and compare those results to the physical experiment. Significant differences in the implant-bone contact area might explain the results of this project and might be a future measurement for geometric accuracy of the mesh.

The final suggestion is to test this method with more specimens. Comparing the model to two implant-bone cadavers is a start for a proof-of-concept. The process of transforming a CT scan into a simulation-ready model has been practiced and optimized. Moving forward, more specimens should be scanned and simulated to prove the effectiveness and accuracy of the model. Furthermore, the strains measured on the buccal and lingual surfaces might be measured with a third method in addition to digital volume correlation and the finite element method (i.e. strain gauges).

Chapter 5

CONCLUSION

In this work, several finite element models were successfully created from micro-CT scans for implant-bone complexes to simulate immediately loaded dental implants. The model was simulated using two mesh sizes and various material properties that provided insights for the effects of these variables on strain in the bone surrounding a dental implant. The finite element method, utilizing a voxel-based mesh, proved to be an adequate technique for measuring strain in the implant-bone complex. Several possible further improvements of the model are suggested. Strain distribution maps, like the ones developed in this project, will advance the research relating bone strain to bone repair. Future dental implants might be designed to achieve the optimal strain for faster healing and stronger implant stability.

Appendix A

Testing Parameters and Results Summary

Implant	Mesh	Cortical Modulus (GPa)	Dentin Modulus (GPa)	Titanium Modulus (GPa)	Buccal Strain	Max Strain	Max Strain Location	Implant Displacement, Top
23	Coarse	15	18.6	116	0.0368%	0.487%	Implant Socket, Upper	12.05
23	Fine	15	18.6	116	0.0360%	0.476%	Implant Socket, Middle	10.92
23	Fine	15	12	116	0.0360%	0.456%	Implant Socket, Middle	11.20
23	Fine	20	18.6	116	0.0280%	0.348%	Implant Socket, Middle	9.20
23	Fine	25	18.6	116	0.0220%	0.259%	Implant Socket, Middle	8.12
23	Fine	15	18.6	90	0.0350%	0.467%	Implant Socket, Middle	11.93
23	Fine	17.5	18.6	116	0.0310%	0.402%	Implant Socket, Middle	9.95
23	Fine	22.5	18.6	116	0.0240%	0.313%	Implant Socket, Middle	8.61
23	Fine	15	18.6	100	0.0360%	0.4494%	Implant Socket, Middle	11.6
26	Fine	15	18.6	116	0.0489%	1.03%	Implant Socket, Middle	18.74
26	Fine	15	12	116	0.0489%	1.03%	Implant Socket, Middle	19.10
26	Fine	17.5	18.6	116	0.0410%	0.89%	Implant Socket, Middle	17.1
26	Fine	20	18.6	116	0.0345%	0.79%	Implant Socket, Middle	15.8
26	Fine	22.5	18.6	116	0.0310%	0.70%	Implant Socket, Middle	14.8
26	Fine	25	18.6	116	0.0270%	0.65%	Implant Socket, Middle	13.9

BIBLIOGRAPHY

[1] J. Du *et al.*, "Biomechanics and strain mapping in bone as related to immediately-loaded dental implants," *J. Biomech.*, vol. 48, no. 12, pp. 3486–3494, 2015.

[2] M. Saini, Y. Singh, P. Arora, V. Arora, and K. Jain, "Implant biomaterials: A comprehensive review.," *World J. Clin. cases*, vol. 3, no. 1, pp. 52–7, 2015.

[3] R. M. Wazen, J. A. Currey, H. Guo, J. B. Brunski, J. A. Helms, and A. Nanci, "Micromotion-induced strain fields influence early stages of repair at bone–implant interfaces," *Acta Biomater.*, vol. 9, no. 5, pp. 6663–6674, 2013.

[4] D. Zhang and Z. Lei, *Emerging Trends in Oral Health Sciences and Dentistry*. CC BY 3.0 license, 2015.

[5] D. Lesmes and Z. Laster, "Innovations in Dental Implant Design for Current Therapy," *Oral and Maxillofacial Surgery Clinics of North America*, vol. 23, no. 2. pp. 193–200, 2011.

[6] L. Le Guéhennec, A. Soueidan, P. Layrolle, and Y. Amouriq, "Surface treatments of titanium dental implants for rapid osseointegration," *Dental Materials*, vol. 23, no. 7. pp. 844–854, 2007.

[7] L. T. de Jonge *et al.*, "The osteogenic effect of electrosprayed nanoscale collagen/calcium phosphate coatings on titanium," *Biomaterials*, vol. 31, no. 9, pp. 2461–2469, 2010.

[8] "EuropeImplant.com Catalog." [Online]. Available: http://www.europeimplant.com/camlog_implants.php. [Accessed: 04-Feb-2017].

[9] D. O'Sullivan, L. Sennerby, and N. Meredith, "Measurements comparing the initial stability of five designs of dental implants: a human cadaver study.," *Clin. Implant Dent. Relat. Res.*, vol. 2, no. 2, pp. 85–92, 2000.

[10] K. Akça, M. Akkocaoglu, A. Cömert, I. Tekdemir, and M. C. Cehreli, "Bone strains around immediately loaded implants supporting mandibular overdentures in human cadavers.," *Int. J. Oral Maxillofac. Implants*, vol. 22, no. 1, pp. 101–9, 2007.

[11] D. T. Reilly and A. H. Burstein, "The Mechanical Properties of Cortical Bone," *J. Bone Jt. Surg.*, vol. 56, no. 5, pp. 1001–1022, 1974.

[12] J. Y. Rho, T. Y. Tsui, and G. M. Pharr, "Elastic properties of human cortical and trabecular lamellar bone measured by nanoindentation," *Biomaterials*, vol. 18, no. 20, pp. 1325–1330, 1997.

[13] Y.-R. Zhang, W. Du, X.-D. Zhou, and H.-Y. Yu, "Review of research on the mechanical properties of the human tooth.," *Int. J. Oral Sci.*, no. 14, pp. 1–9, 2014.

[14] R. B. Anchieta *et al.*, "Mechanical property assessment of bone healing around a titanium-zirconium alloy dental implant," *Clin. Implant Dent. Relat. Res.*, pp. 913–919, 2014.

ACADEMIC VITA

Academic Vita of Ryan Shannon
rshannon102@gmail.com

EDUCATION

The Pennsylvania State University
Bachelor's Degree in Mechanical Engineering
with Minors in Mathematics and Statistics
with Honors in Mechanical Engineering from the Schreyer's Honors College

Thesis Title: A Computational Analysis of the Biomechanics of Immediately Loaded Dental Implants
Thesis Supervisor: Dr. Jing Du, Assistant Professor of Mechanical Engineering

WORK EXPERIENCE

Summer 2016
Vehicle Safety, Data Scientist Intern
Identify potential safety issues with automotive fleet using data analytics tools
General Motors Company, Warren MI
Carolyn Nguyen

Summer 2014, Summer 2015
Vehicle Occupant Safety Research Intern
Develop finite element occupant models and reconstruct vehicle crash events for model validation
Wake Forest University, Winston-Salem NC
Dr. Scott Gayzik, Dr. Ashley Weaver

AWARDS

Louis A. Harding Memorial Scholarship from the Department of Mechanical and Nuclear Engineering at The Pennsylvania State University (2015)
The Pennsylvania State University President Sparks Award for General Excellence as a Sophomore (2015)
The Pennsylvania State University President's Freshman Award (2014)

PUBLICATIONS

Ranslow Allison N., Kraft Reuben H., Shannon Ryan, et al.
"Microstructural Analysis of Porcine Skull Bone Subjected to Impact Loading". ASME. ASME International Mechanical Engineering Congress and Exposition, Volume 3: Biomedical and Biotechnology Engineering ():V003T03A057. doi:10.1115/IMECE2015-51979.